Unified Model for Transient Faradaic Impedance Spectroscopy: Theory and Prediction

1 AUTHOR:

Qiu-An Huang
Hubei University
11 PUBLICATIONS **219** CITATIONS

Unified Model for Transient Faradaic Impedance Spectroscopy: Theory and Prediction

Qiu-An Huang[†] and Su-Moon Park*

Interdisciplinary School of Green Energy, Ulsan National Institute of Science and Technology, Ulsan 689-805, Korea

ⓢ Supporting Information

Charge (G_p) and Mass (Y_W) Transfer Admittances and Their Evolution
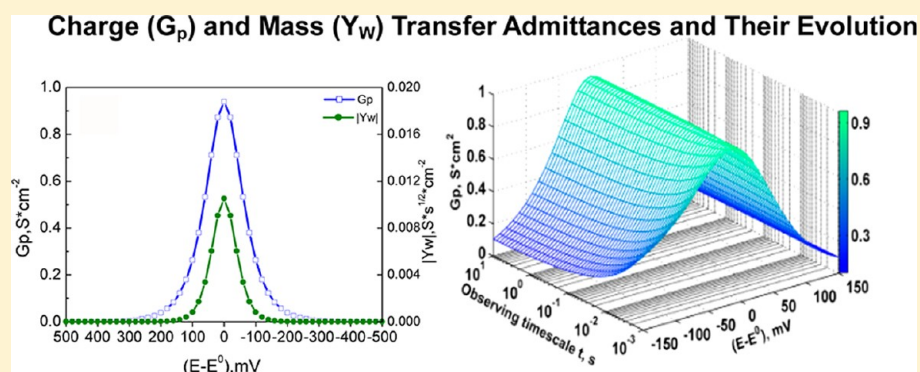
ABSTRACT: We describe a unified model for transient faradaic impedance spectroscopy developed by obtaining a rigorous expression for the current for a potential step to an electrochemical system containing an oxidant and/or a reductant with no assumptions on the reversibility for redox reactions. Effects of electrode reaction kinetic and other parameters such as the exchange rate constant (k^0), potential step period (t_p), diffusion coefficient (D), transfer coefficient (α), the number of electrons transferred (n), and overpotential (η) on observed impedance parameters have been evaluated using the model. We obtained both polarization resistances (R_p's) and Warburg impedances (Z_w's) to characterize the nature of the charge-transfer reaction by showing the evolution trend in terms of their admittances employing kinetic parameters such as η, k^0, t_p, a, n, and D. The peak shift and the half-peak width of Warburg admittance voltammograms were also studied as a function of k^0. We finally discuss ranges of step periods, which allow meaningful transient impedance measurements to monitor faradaic processes in real-time by staircase cyclic voltammetric-Fourier transform electrochemical impedance spectroscopy (SCV-FTEIS) experiments, for a given step height.

INTRODUCTION

Electrochemical impedance spectroscopy (EIS) is the only viable way that allows a complete description to be made on an electrochemical system when properly conducted and interpreted.[1−4] This is because it provides all the information necessary to describe the electrified interface including faradaic and nonfaradaic processes along with that associated with the electrolyte solution. Information that can be obtained by EIS measurements on the faradaic process includes both its thermodynamics (standard or formal potentials) and charge as well as mass-transfer kinetics.[5,6] Comprehensive information can be obtained only by analysis of a large body of impedance data acquired as a function of potential and/or time by transient impedance measurements.[5,6] For this reason, a variety of EIS measurement methods have been developed over the years.

The frequency response analyzer (FRA) is currently the state-of-the-art method of impedance measurements.[7] It is, however, configured to make the measurements after the machine waits until a steady state current is obtained to meet the stationarity and causality requirements.[8−11] It is thus difficult, if not impossible, to contiguously obtain impedance data as a function of potential by this technique. Besides, the technique misses the information in an earlier part of the potential step to set a dc bias for electrolysis. To resolve this problem, efforts have been made from as early as in 1970s by Smith et al.,[12] in which a multisine signal obtained by mixing a number of ac voltages of various frequencies was used and the resulting current was converted to ac currents of the corresponding frequencies. The impedances were then obtained for frequencies used to assemble the composite signal after the current signal was deconvoluted by fast Fourier transform. The technique is thus rightly termed the Fourier transform electrochemical impedance spectroscopy (FTEIS). The FTEIS method based on multisine excitation signals has recently been improved by a few investigators,[13−16] but it is still not without a few limitations such as it cannot be used at a voltage scan rate above 5 mV/s.[16] For transient impedance measurements, Gabrieli et al.[17] later proposed the use of step

signals and concluded that it may be used in a narrow frequency range in the lower frequency part as its analysis accuracy was lower in the high frequency region than for white noise and sine wave perturbation. Mochalov and Kolosnitsyn then used the galvanostatic step for the EIS measurements in a frequency range of 1 mHz through 300 kHz.[18] By then, a new form of the FTEIS method appeared, in which a small potential step was used as an integrated form of a true white noise perturbation signal, i.e., the Dirac δ function, followed by conversion of derivative signals of the stepped potential and the resultant current into ac voltages and currents in a frequency range from $1/t_p$ to $1/2\Delta t$, where t_p is the step period and Δt is the sampling interval, leading to a full frame impedance spectrum.[19] This neo-FTEIS method was developed into a real-time measurement technique during a potential sweep by combining it with the staircase cyclic voltammetric (SCV) experiment,[5] which led to a large body of information at a large number of dynamic bias potentials with 5−25 mV intervals, making full descriptions of a variety of electrochemical systems possible.[20]

In this study, we develop a unified model for transient EIS without assuming the reversibility of the electron-transfer reaction for SCV-FTEIS experiments. On the basis of the model, evolution of the faradaic and mass-transfer impedances is obtained and described in the form of their respective admittances using related electrode kinetic parameters such as k^0, t_p, D, a, n, and η. The range of t_p, during which reliable transient impedance measurements can be made using SCV-FTEIS, are provided for different ranges of exchange rate constants as well as diffusion coefficients.

■ THEORETICAL CONSIDERATIONS

1. Faradaic and Nonfaradaic Currents. When a potential step is applied to a working electrode in a solution containing a redox pair, O and R, we expect to have an electrochemical reaction,

$$O + n\mathrm{e} \underset{k_b}{\overset{k_f}{\rightleftarrows}} R \tag{1}$$

The faradaic current has the following expression under an experimental condition described by the semi-infinite diffusion,[21]

$$i_F(t) = nFA(k_f C_O^* - k_b C_R^*) \exp(H^2 t)\, \mathrm{erfc}(Ht^{1/2}) \tag{2}$$

with

$$H = \frac{k_f}{D_O^{1/2}} + \frac{k_b}{D_R^{1/2}} \tag{3}$$

Here C_O^* and C_R^* are the bulk concentrations for O and R, k_f and k_b are the forward and backward rate constants for electrochemical reaction 1, D_O and D_R are the diffusion coefficients for O and R, F is the faraday constant, A is the electrode surface area, and n is the number of electrons transferred for reaction 1. Relation 2 perfectly describes the faradaic current for reaction 1 except for the nonfaradaic currents due to double-layer charging and the uncompensated resistance. A more complete current expression including both faradaic and nonfaradaic components has been obtained by taking advantage of the Randles equivalent circuit.[19,22,23]

Let us now apply a potential step, $U(s)$, to the Randles circuit shown in Figure 1 as an input signal in a complex frequency field,
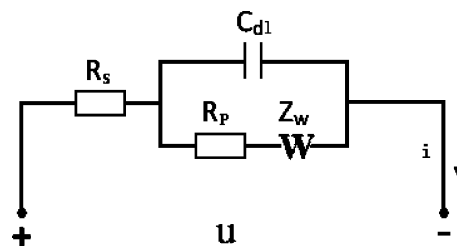
$$U(s) = \frac{\Delta E}{s} \tag{4}$$

Figure 1. Classical Randles circuit. Here, R_s is the uncompensated solution electrolyte resistance, R_p is the activation polarization resistance, Z_w is the Warburg impedance, and C_{dl} is the double layer capacitance.
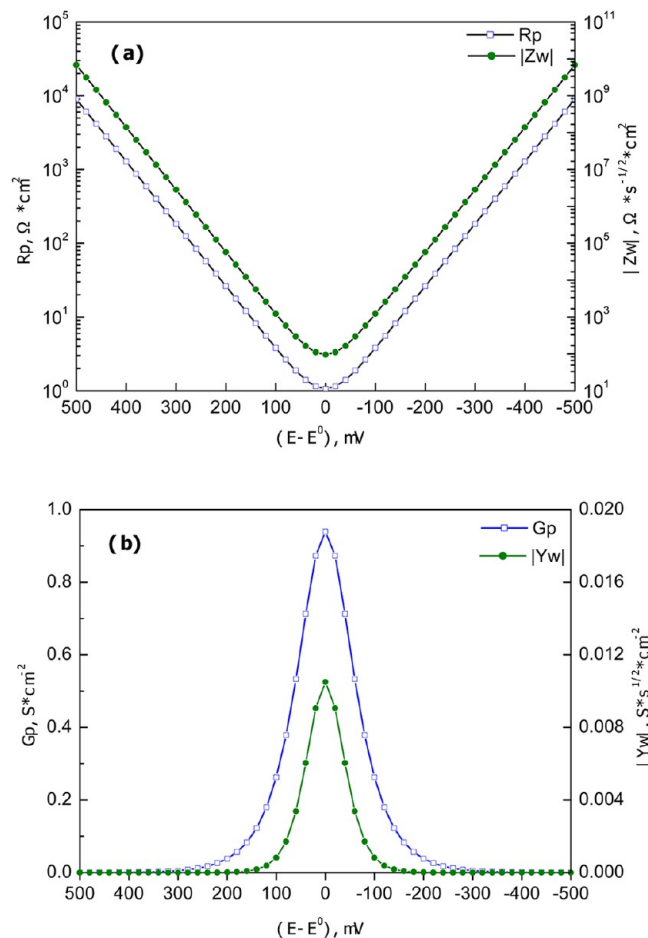

Figure 2. (a) R_p and Z_w vs η and (b) G_p (conductance) and Y_w (Warburg admittance) plots for a reversible case.

where s is complex frequency and ΔE is the amplitude of the potential step. The mass-transfer impedance, Z_w, is written as[24,25a]

$$Z_w(s) = \frac{\sqrt{2}\,\sigma_t}{\sqrt{s}} \tag{5}$$

where σ_t is the mass-transfer coefficient. The total impedance in the complex frequency domain is then[26]

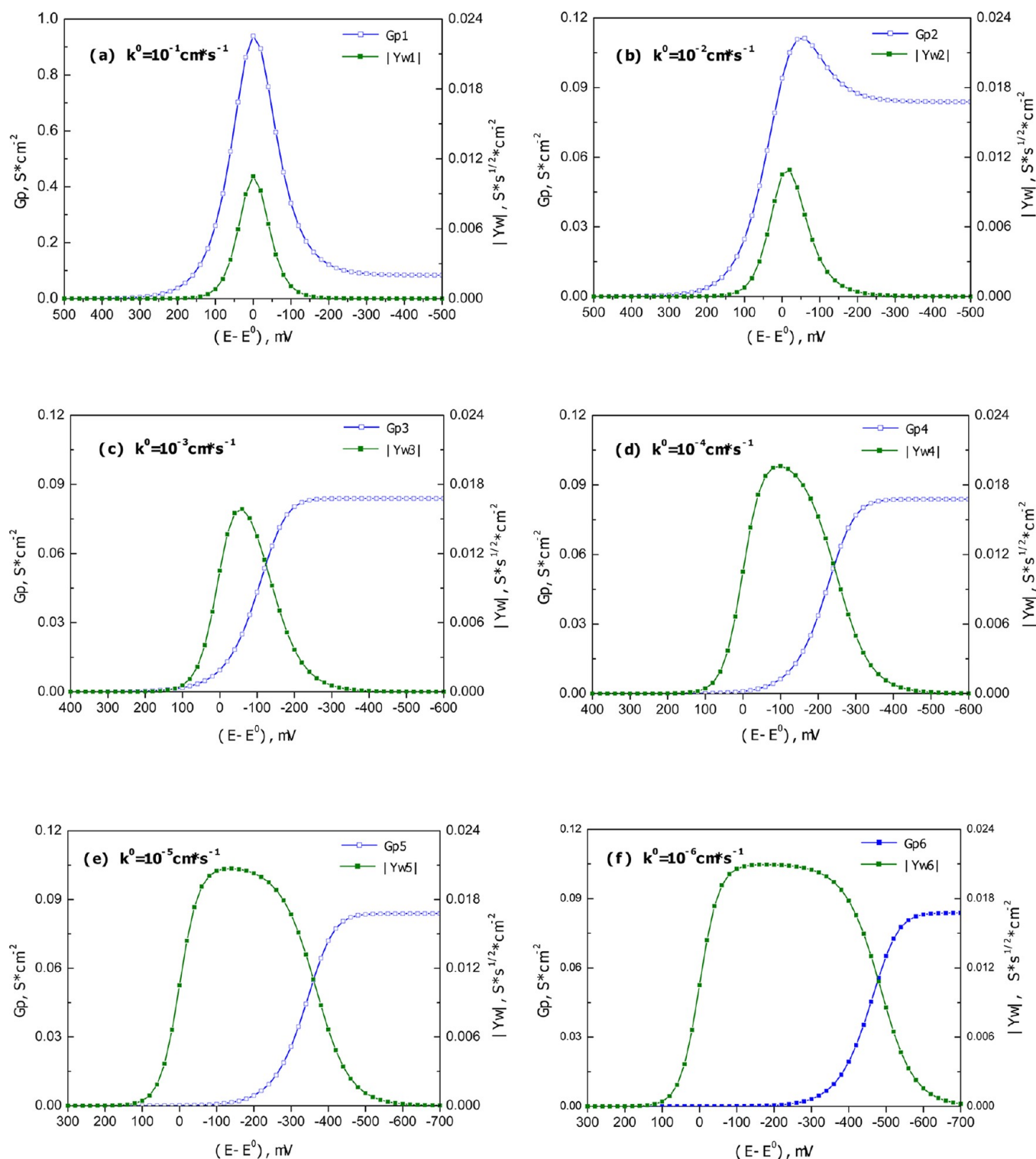$$Z(s) = R_s + \frac{R_p + \frac{\sqrt{2}\,\sigma_t}{\sqrt{s}}}{1 + sC_{dl}R_p + sC_{dl}\frac{\sqrt{2}\,\sigma_t}{\sqrt{s}}} \tag{6}$$

Figure 3. Effects of exchange rate constants on polarization conductance (□) and Warburg admittance (■) plotted as a function of overpotential for $D_O = D_R = 5 \times 10^{-6}$ cm^2/s and $t_p = 0.02$ s. The k^0 values are (a) 1×10^{-1}, (b) 1×10^{-2}, (c) 1×10^{-3}, (d) 1×10^{-4}, (e) 1×10^{-5}, and (f) 1×10^{-6} cm/s, respectively.

We thus obtain the current expression in complex frequency field as

$$I(s) = \frac{\Delta E}{R_s R_p C_{dl} \sqrt{s}} \cdot \frac{R_p C_{dl} s + \sqrt{2}\sigma_t \sqrt{s} + 1}{(\sqrt{s})^3 + \frac{\sqrt{2}\sigma_t}{R_p}s + \frac{R_s + R_p}{R_s R_p C_{dl}}\sqrt{s} + \frac{\sqrt{2}\sigma_t}{R_s R_p C_{dl}}}$$

(7)

This equation contains all the parameters including charge and mass transfer as well as nonfaradaic components, which are necessary to describe a charge-transfer reaction at the electrode/electrolyte interface. The impedance data measured by an SCV-FTEIS experiment should then contain all the kinetic information as it contains a series of ascending and/or descending steps. In the present work, we focus our discussion on

developing a transient faradaic impedance model suitable for the SCV-FTEIS experiment.

2. Unified Model for Transient Faradaic Impedance Spectroscopy.

We now develop a model for the transient faradaic impedance without assuming the reversibility of reaction 1 for the SCV-FTEIS impedance measurement platform.

Phasor Operation and Small-signal Perturbation Method. On the basis of the previous work on the faradaic impedance model,[24] we incorporate a phasor operation for a small-signal perturbation to clarify a few key concepts such as reversibility and linearity. When a small potential step, $E(t)$, is applied to redox reaction 1, we obtain a faradaic current expression,[25b]

$$I_F(t) = nFA(k_f C_O(0,t) - k_b C_R(0,t)) \tag{8-1}$$

where

$$k_f = k^0 \exp(-\alpha nf(E(t) - E^{0'})) \tag{8-2}$$

and

$$k_b = k^0 \exp[(1 - \alpha)nf(E(t) - E^{0'})] \tag{8-3}$$

with

$$f = \frac{F}{RT} \tag{8-4}$$

For a small ac perturbation signal, $\Delta u(t)$, applied to the dc bias potential, E_{dc}, both the perturbation and its response can be linearized. Hence, they have the following expressions:

$$E(t) = E_{dc} + \Delta u(t) \tag{9-1}$$

$$I_F(t) = I_{dc} + \Delta i(t) \tag{9-2}$$

$$C_O(x,t) = C_{O,dc} + \Delta c_O(x,t) \tag{9-3}$$

$$C_R(x,t) = C_{R,dc} + \Delta c_R(x,t) \tag{9-4}$$

and

$$\Delta u(t) = \Delta U \cdot e^{j(\omega t + \phi_u)} \xrightarrow{\overline{\Delta U} = \Delta U \cdot e^{j\phi_u}} \overline{\Delta U} \cdot e^{j\omega t} \tag{10-1}$$

$$\Delta i_F(t) = \Delta I_F \cdot e^{j(\omega t + \phi_i)} \xrightarrow{\overline{\Delta I_F} = \Delta I_F \cdot e^{j\phi_i}} \overline{\Delta I_F} \cdot e^{j\omega t} \tag{10-2}$$

$$\Delta c_O(x,t) = \Delta C_O(x) \cdot e^{j(\omega t + \phi_{C_O})} \xrightarrow{\overline{\Delta C_O}(x) = \Delta C_O(x) \cdot e^{j\phi_{C_O}}} \overline{\Delta C_O}(x) \cdot e^{j\omega t} \tag{10-3}$$

$$\Delta c_R(x,t) = \Delta C_R(x) \cdot e^{j(\omega t + \phi_{C_R})} \xrightarrow{\overline{\Delta C_R}(x) = \Delta C_R(x) \cdot e^{j\phi_{C_R}}} \overline{\Delta C_R}(x) \cdot e^{j\omega t} \tag{10-4}$$

Here $\overline{\Delta U}$, $\overline{\Delta I_F}$, $\overline{\Delta C_O}(x)$, and $\overline{\Delta C_R}(x)$ denote corresponding phasors of the perturbed voltage, current, and respective concentrations of O and R. Similarly, φ_u, φ_i, φ_{C_O}, and φ_{C_R} denote the corresponding initial phase angles.

The current expression may also be represented by Taylor's series of just the first-order terms with higher order terms ignored as shown below:

$$\Delta i_F(t) = \frac{\partial I_F(t)}{\partial E(t)} \Delta u(t) + \frac{\partial I_F(t)}{\partial C_O(0,t)} \Delta c_O(0,t) + \frac{\partial I_F(t)}{\partial C_R(0,t)} \Delta c_R(0,t) \tag{11}$$

We point out that the small-signal perturbation guarantees the expression, $\Delta i_F(t)$, in a tolerable error range by ignoring

higher order terms; this also serves as a precondition for the linearity of the subsequently derived faradaic impedance model.

Substituting eqs 10-1−10-4 into eq 11, we obtain

$$\overline{\Delta I_F} = \frac{\partial I_F(t)}{\partial E(t)} \overline{\Delta U} + \frac{\partial I_F(t)}{\partial C_O(0,t)} \overline{\Delta C_O}(0) + \frac{\partial I_F(t)}{\partial C_R(0,t)} \overline{\Delta C_R}(0) \tag{12}$$

Here we obtain $\partial I_F(t)/\partial E(t)$, $\partial I_F(t)/\partial C_O(0,t)$, and $\partial I_F(t)/\partial C_R(0,t)$ from eq 8. Both $\overline{\Delta C_O}(0)$ and $\overline{\Delta C_R}(0)$ are obtained by solving Fick's diffusion equations under semi-infinite diffusion conditions.[24,25c] Now, we define faradaic impedance, Z_F, as

$$Z_F \equiv -\frac{\overline{\Delta U}}{\overline{\Delta I_F}}$$

$$= \frac{RT}{n^2 F^2 A[\alpha k_f C_O(0,t) + (1 - \alpha)k_b C_R(0,t)]}$$
$$\cdot \left(1 + \frac{k_f}{\sqrt{j\omega D_O}} + \frac{k_b}{\sqrt{j\omega D_R}}\right) \tag{13}$$

The faradaic impedance, $Z_F \equiv R_p + Z_w$, consists of the polarization resistance, R_p, during charge transfer and the Warburg impedance due to mass transfer of both O and R, $Z_w \equiv Z_{w,O} + Z_{w,R}$. Considering k_f and k_b given by eqs 8-2 and 8-3, R_p, $Z_{w,O}$, and $Z_{w,R}$ are expressed as follows:

$$R_p = \frac{RT}{n^2 F^2 A} \cdot \frac{e^{\alpha nf[E(t) - E^{0'}]}}{k^0[\alpha C_O(0,t) + (1 - \alpha)e^{nf[E(t) - E^{0'}]}C_R(0,t)]} \tag{14-1}$$

$$Z_w \equiv Z_{w,O} + Z_{w,R} \tag{14-2}$$

$$Z_{w,O} = \frac{RT}{n^2 F^2 A \sqrt{j\omega D_O}} \cdot \frac{1}{[\alpha C_O(0,t) + (1 - \alpha)e^{nf[E(t) - E^{0'}]}C_R(0,t)]} \tag{14-3}$$

and

$$Z_{w,R} = \frac{RT}{n^2 F^2 A \sqrt{j\omega D_R}} \cdot \frac{e^{nf[E(t) - E^{0'}]}}{[\alpha C_O(0,t) + (1 - \alpha)e^{nf[E(t) - E^{0'}]}C_R(0,t)]} \tag{14-4}$$

The general mass-transfer coefficients have also respective expressions as

$$Z_w \equiv \frac{\sqrt{2}\,\sigma_t}{\sqrt{j\omega}} \tag{15-1}$$

$$\sigma_t = \sigma_O + \sigma_R \tag{15-2}$$

$$\sigma_O \equiv \frac{RT}{n^2 F^2 A \sqrt{2D_O}} \cdot \frac{1}{\alpha C_O(0,t) + (1 - \alpha)e^{nf[E(t) - E^{0'}]}C_R(0,t)} \tag{15-3}$$

and

D

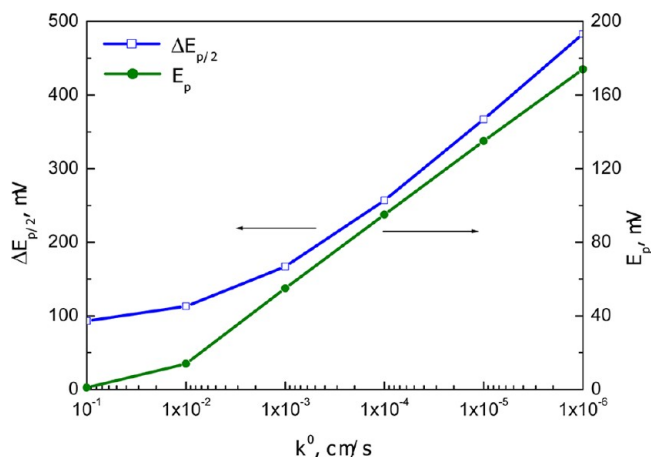dx.doi.org/10.1021/jp306140w | J. Phys. Chem. C XXXX, XXX, XXX−XXX

Figure 4. Warburg admittance peak potentials (E_p) and half-peak widths ($\Delta E_{p/2}$) plotted from the data shown in Figure 3.
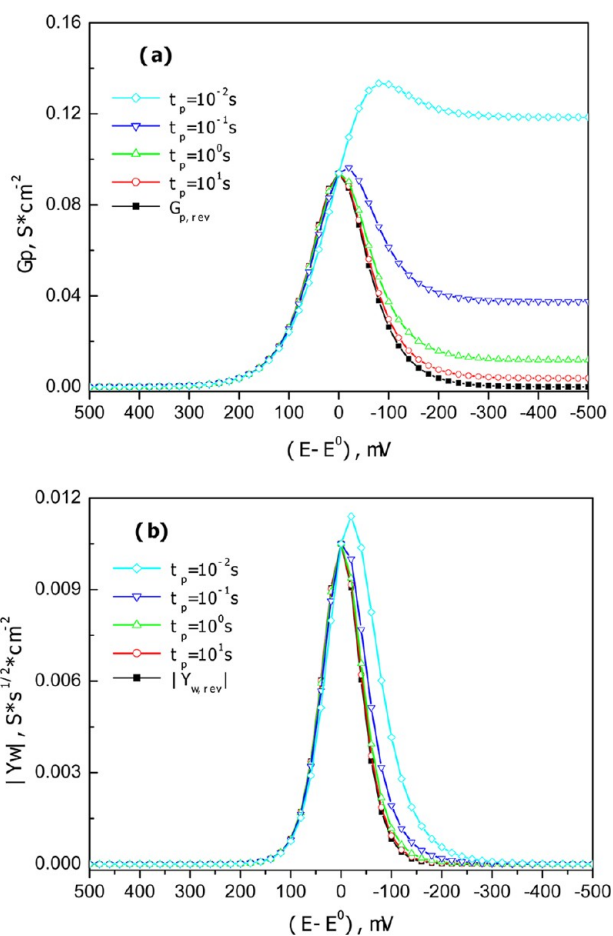

Figure 5. Effects of t_p on G_p (a) and Y_w (b) plotted as a function of η for $k^0 = 0.01$ cm/s and $D = 5 \times 10^{-6}$ cm^2/s. The t_p values were varied from 0.01 to 10 s with $G_{p,rev}$ and $Y_{w,rev}$ for the reversible case.

$$\sigma_R \equiv \frac{RT}{n^2 F^2 A \sqrt{2D_R}}$$

$$\cdot \frac{e^{nf[E(t)-E^{0'}]}}{\alpha C_O(0,t) + (1-\alpha)e^{nf[E(t)-E^{0'}]}C_R(0,t)} \qquad (15\text{-}4)$$

Because the above faradaic impedance expressions were derived without reference to the reversibility and equilibrium of
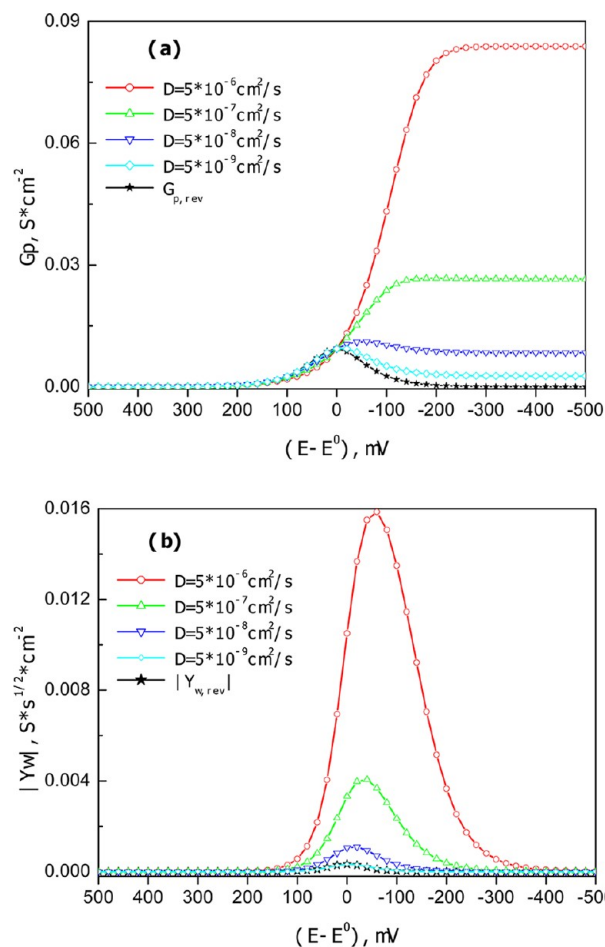

Figure 6. Effects of D on G_p (a) and Y_w (b) plotted as a function of η for $k^0 = 0.001$ cm/s, $D = 5 \times 10^{-6}$ cm^2/s, and $t_p = 20$ ms. The D value was varied from 5×10^{-6} to 5×10^{-9} cm^2/s and $G_{p,rev}$ and $Y_{w,rev}$ represent those for the reversible case.

reaction 1, they hold for reversible, quasi-reversible, and irreversible electrochemical systems, as well as for stationary and nonstationary systems. As a consequence, we regard them as unified models for transient faradaic impedance. It is not possible, however, to directly apply the models to impedance data analysis due to intermediate variables such as $C_O(0,t)$ and $C_R(0,t)$. Now we address the problem of eliminating these parameters and express the equations using a few experimental parameters including t, D, k^0, and η $[\equiv E(t) - E^0]$.

Now let us examine the unified model for analysis and diagnosis of transient impedance data obtained by SCV-FTEIS experiments under various reversibility conditions. A staircase cyclic voltammogram (SCV) is obtained by simply connecting a series of currents sampled at sampling time, t_s, during each ascending and/or descending step; the SCV is the same as the cyclic voltammogram (CV) recorded at a scan rate of $\Delta E/t_s$, where ΔE is the potential step height as defined above.[27] In this work, t_s is synchronous with the step period, t_p, as t_s is taken as the end of the potential step. Thus, both the CV and potentiodynamic impedance data are simultaneously obtained at various dc biases and scan rates employing the SCV experiments.[20]

Reversible Cases. For a reversible case, the surface concentrations are described by the Nernst equation,

E

dx.doi.org/10.1021/jp306140w | J. Phys. Chem. C XXXX, XXX, XXX−XXX

$$\theta = \frac{k_b}{k_f} = \frac{C_O(0,t)}{C_R(0,t)} = e^{nf[E(t)-E^{0'}]} \tag{16}$$

Although only O is initially present in the solution,[24,25] R is generated during the series of incrementing/decrementing potential steps during SCV-FTEIS experiments and their surface concentrations are expressed as[24,25]

$$C_O(0,t) = C_O^* \frac{\xi\theta}{1+\xi\theta} \tag{17-1}$$

$$C_R(0,t) = C_O^* \frac{\xi}{1+\xi\theta} \tag{17-2}$$

where

$$\theta = e^{nf[E(t)-E^{0'}]} \tag{17-3}$$

$$\xi = (D_O/D_R)^{1/2} \tag{17-4}$$

and

$$E_{1/2} = E^{0'} + \frac{RT}{nF}\ln\left[\frac{D_R^{1/2}}{D_O^{1/2}}\right] \tag{17-5}$$

Substituting eqs 17 into eqs 14 followed by appropriate arrangements, we obtain the following impedance equations:

$$R_{p,rev} = \frac{RT}{n^2F^2AC_O^*k^0\xi^\alpha} \frac{1+e^{nf[E(t)-E_{1/2}]}}{e^{(1-\alpha)nf[E(t)-E_{1/2}]}} \tag{18-1}$$

and

$$Z_{w,rev} = \frac{4RT}{n^2F^2AC_O^*\sqrt{j\omega D_O}} \cdot \cosh^2\left[\frac{nf[E(t)-E_{1/2}]}{2}\right] \tag{18-2}$$

Thus, the R_p value has the following minimum value at $E_s \equiv E_{1/2} - RT/nF \ln[\alpha/(1-\alpha)]$,

$$(R_{p,rev})_{\min|E_s} = \frac{RT}{n^2F^2AC_O^*k^0\xi^\alpha} \frac{1}{\alpha^\alpha(1-\alpha)^{1-\alpha}} \tag{19-1}$$

Similarly, the Warburg impedance has its minimum value at $E = E_{1/2}$,

$$(Z_{w,rev})_{\min|E_{1/2}} = \frac{4RT}{n^2F^2AC_O^*\sqrt{\omega D_O}} \tag{19-2}$$

Quasi-Reversible Cases. The quasi-reversible system represents a general case as its one extreme is the reversible case whereas the other represents the totally irreversible one. For this reason, a quasi-reversible case can be straightforwardly converted to a reversible or irreversible one depending on the conditions.[28] For a quasi-reversible case, we need to use the Butler–Volmer formalism for one of its boundary conditions to solve Fick's diffusion equations; we obtain the following concentration profiles after a series of mathematical operations including the Laplace transformation:[25c,29]

$$C_O(0,t) = C_O^*\left\{1 - \frac{k_f}{HD_O^{1/2}}\left[1 - e^{(H\sqrt{t})^2}\mathrm{erfc}(H\sqrt{t})\right]\right\} \tag{20-1}$$

and

$$C_R(0,t) = C_O^* \frac{k_f}{HD_R^{1/2}}\left[1 - e^{(H\sqrt{t})^2}\mathrm{erfc}(H\sqrt{t})\right] \tag{20-2}$$

Substitution of these expressions into R_p and σ expressions (eqs 14-1, 15-3, and 15-4), we obtain the following *unified* formalisms:

$$R_{p,qr} = \frac{RT}{n^2F^2Ak^0C_O^*} \frac{e^{\alpha nf[E(t)-E^{0'}]}}{\alpha\left\{1 - \frac{k_f}{HD_O^{1/2}}\left[1 - e^{(H\sqrt{t})^2}\mathrm{erfc}(H\sqrt{t})\right]\right\} + (1-a)\frac{k_f}{HD_R^{1/2}}\left[1 - e^{(H\sqrt{t})^2}\mathrm{erfc}(H\sqrt{t})\right]e^{nf[E-E^{0'}]}} \tag{21-1}$$

$$\sigma_{O,qr} \equiv \frac{RT}{n^2F^2AC_O^*\sqrt{2D_O}} \frac{1}{\alpha\left\{1 - \frac{k_f}{HD_O^{1/2}}\left[1 - e^{(H\sqrt{t})^2}\mathrm{erfc}(H\sqrt{t})\right]\right\} + (1-a)\frac{k_f}{HD_R^{1/2}}\left[1 - e^{(H\sqrt{t})^2}\mathrm{erfc}(H\sqrt{t})\right]e^{nf[E-E^{0'}]}} \tag{21-2}$$

$$\sigma_{R,qr} \equiv \frac{RT}{n^2F^2AC_O^*\sqrt{2D_R}} \frac{e^{nf[E(t)-E^{0'}]}}{\alpha\left\{1 - \frac{k_f}{HD_O^{1/2}}\left[1 - e^{(H\sqrt{t})^2}\mathrm{erfc}(H\sqrt{t})\right]\right\} + (1-a)\frac{k_f}{HD_R^{1/2}}\left[1 - e^{(H\sqrt{t})^2}\mathrm{erfc}(H\sqrt{t})\right]e^{nf[E(t)-E^{0'}]}} \tag{21-3}$$

Further, we obtain $Z_{w,qr}$ from eq 15-1 and eq 15-2

$$Z_{w,qr} = \frac{\sqrt{2}(\sigma_{O,qr} + \sigma_{R,qr})}{\sqrt{j\omega}} \tag{21-4}$$

As can be seen from these relations, it is not trivial to conclude much about how the overall impedances would behave depending on various input parameters. We point out

though that the expressions, which have not been described in the literature, are applicable to all cases. The evolution trends of transient faradaic impedances we describe below allow proper experimental parameters to be set for reliable transient impedance measurements for different reversibility cases.
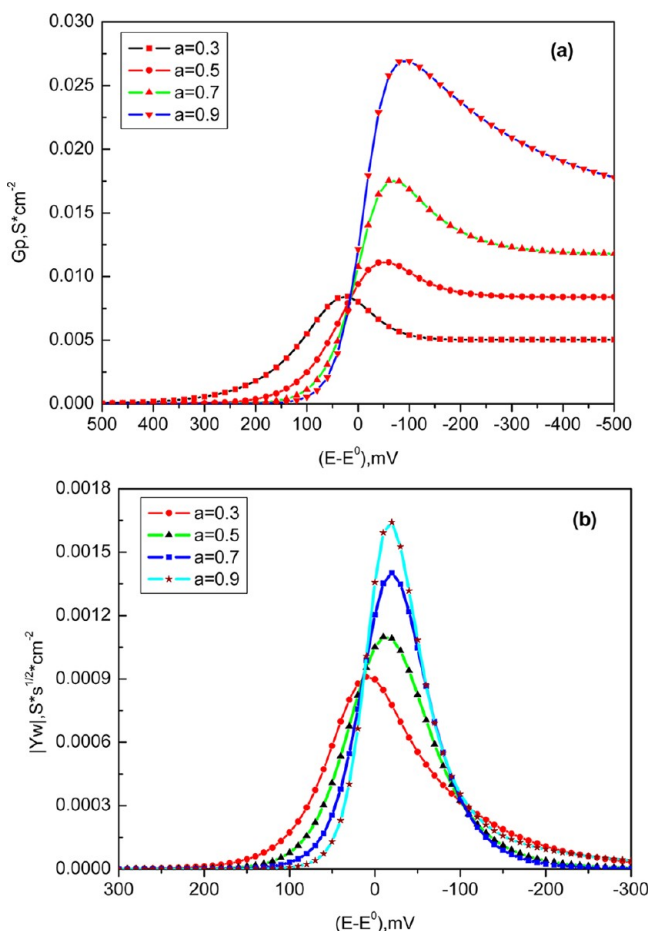
Figure 7. Effects of α on G_p (a) and Y_w (b) plotted as a function of η for $k^0 = 0.001$ cm/s, $D = 5 \times 10^{-8}$ cm^2/s, $n = 1.0$, and $t_p = 20$ ms. The α value was varied from 0.3 to 0.9.

Figure 8. Effects of n on G_p (a) and Y_w (b) plotted as a function of η for $k^0 = 0.001$ cm/s, $D = 5 \times 10^{-8}$ cm^2/s, $\alpha = 0.5$, and $t_p = 20$ ms. The n value was varied from 1.0 to 3.0.

Irreversible Cases. In these cases, only the forward term is considered in the Butler–Volmer equation with the backward term ignored. Thus, all the relations derived for a quasi-reversible system are good except that

$$H = \frac{k_f}{D_O^{1/2}} \tag{22}$$

■ RESULTS AND DISCUSSION

Now, we are ready to examine how faradaic impedances or admittances evolve depending on inherent reaction and experimental parameters including k^0, t, D, α, n, and η. For the computer simulation using the above equations, we use the following parameters in equations for impedances: $T = 298$ K; $A = 1.0$ cm^2; initial bulk concentrations of $C_O^* = 5.0$ mM and $C_R^* = 0$, respectively; and $D_O = D_R$ leading to $E^{0'} = E^0$. Unless otherwise specified, we use $\alpha = 0.50$ and $n = 1.0$ for all calculations. We now examine the impedance/admittance trends shown by the reversible, quasi-reversible, and irreversible cases.

1. Faradaic Impedances/Admittances for Reversible Cases. A reversible electrochemical reaction proceeds so rapidly that equilibrium is reached instantly during the experiment. Figure 2 shows: (a) the impedances and (b) the admittance and conductance plotted as a function of
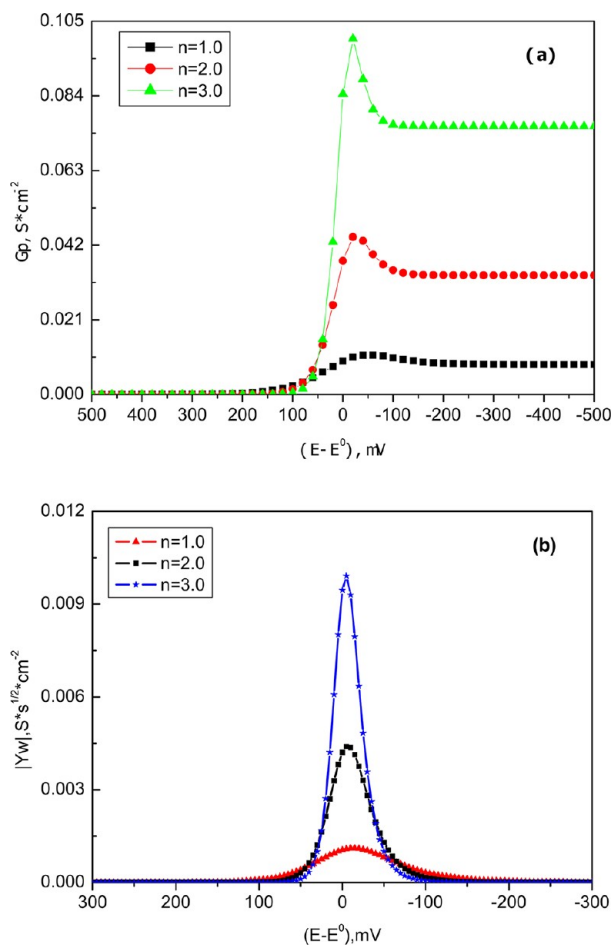
overpotential. Note that the increase and decrease in impedances and admittances are symmetrical with respect to E^0. Also, eqs 18 and 19 predict that Z_w and R_p would go through a minimum or their admittance and conductance values, $Y_w = 1/Z_w$ and $G_p = 1/R_p$, show maximum values at $E = E_{1/2}$. The behavior shown here is in excellent agreement with that reported previously.[30] The maximum Warburg admittance (see Supporting Information) is

$$Y_{w,p} = \frac{n^2 F^2 A C_O^* \sqrt{D}}{4RT} \tag{23}$$

and the half peak width at $Y_{p/2}$ is $\Delta E_{p/2}$ independent of k^0 and t_p in excellent agreement with the one previously reported.[6]

2. Quasi-Reversible Faradaic Admittance Evolution: Effects of k^0. Figure 3 shows G_p and Y_w values as a function of η obtained using eqs 21-1−21-3 for k^0 values ranging from 10^{-1} to 10^{-6} cm/s at $t_p = 20$ ms. As can be seen, the G_p and Y_w plots are almost bell-shaped for $k^0 = 10^{-1}$ cm/s, as was shown for a reversible case in Figure 2. Although the Y_w peak potential shows almost no shift, the $\Delta E_{p/2}$ value is about 93.0 mV, indicating its peak has been broadened albeit slightly. When k^0 becomes smaller, the bell-shaped mass transport admittance plots become increasingly more deformed in comparison to that of the reversible case. The peak shift and broadening depending
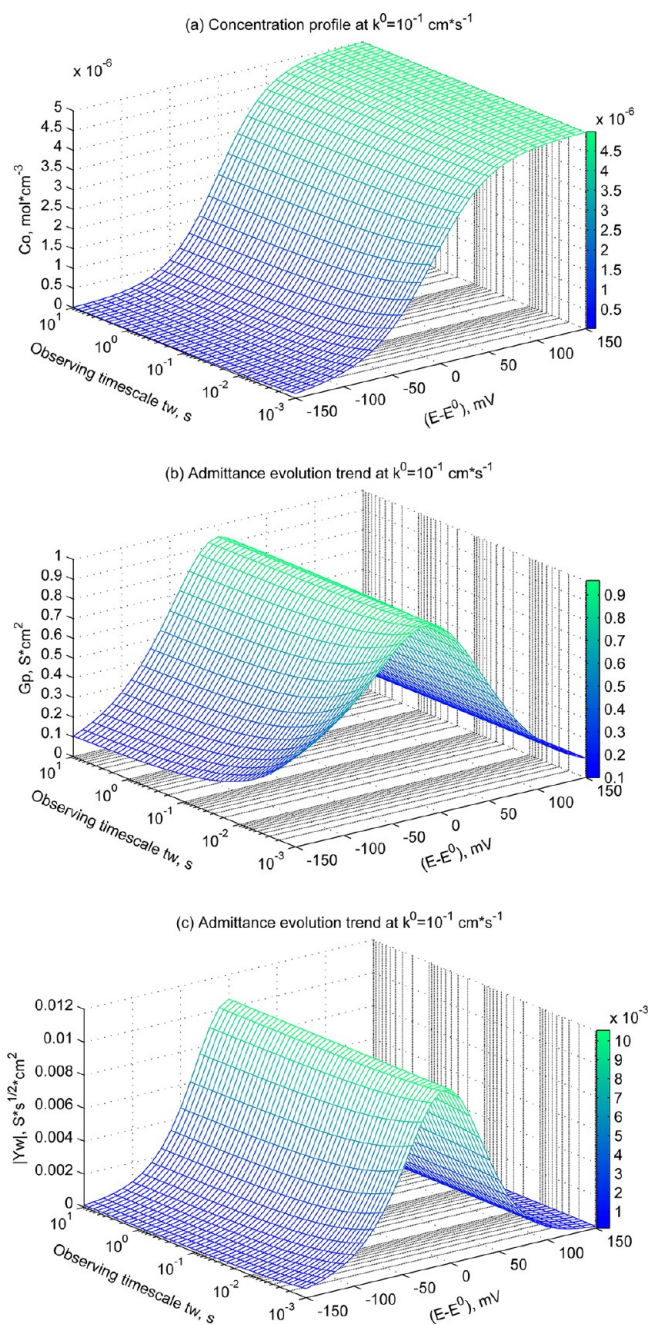
(a) Concentration profile at $k^0=10^{-1}$ cm*s^{-1}

(b) Admittance evolution trend at $k^0=10^{-1}$ cm*s^{-1}

(c) Admittance evolution trend at $k^0=10^{-1}$ cm*s^{-1}

Figure 9. (a) $C_O(x,t)$, (b) G_p, and (c) Y_w plotted as a function of t and η, for a reaction with $k^0 = 0.1$ cm/s and $D = 5 \times 10^{-6}$ cm^2/s.

on k^0 values are summarized in Figure 4, which shows that the Y_w peak potential shifts in a negative direction and $\Delta E_{p/2}$ increases with the decrease in k^0. The shift in its peak potential and the broadening of the Warburg admittance voltammogram for the decreased k^0 values is in general agreement with the experimental result reported earlier,[5] although our current result cannot be quantitatively compared with those reported therein.

Figure 4 shows that the reversibility rapidly deteriorates for the k^0 values smaller than 10^{-1} cm/s. This is because t_p (=20 ms) used for the calculations is too short; for an SCV experiment, this corresponds to a scan rate of 500 mV/s for a 10 mV step height (=10 mV/20 ms), which renders most of reactions dealt with here quasi-reversible or irreversible. In other words, the

experimental conditions used for our simulation was very stringent and the electrochemical system with a k^0 value of 10^{-2} cm/s is regarded to be fairly irreversible under this experimental condition. For longer t_p values, the systems appear more reversible than shown here. We will address more on the effects of t_p below.

Another point we note in Figure 3 is that the G_p vs η plot increasingly becomes the S or sigmoidal shape from the bell shape for the reversible case as k^0 decreases. These behaviors are very similar to the current/potential (I/E) curve shapes of irreversible systems.[25c,31,32] These shapes were observed in the polarographic experiments, which used the small potential steps during the mercury drop period resembling those used in SCV experiments we are describing here.

3. Quasi-Reversible Faradaic Admittance: Effects of t_p. As pointed out above, the step period (t_p) boils down to the voltage scan rate (v) for a given potential step size as $v = \Delta E/t_p$ in a SCV experiment.[27,34] The effect of t_p is thus equivalent to that of the scan rate on the impedance parameters obtained by the SCV experiment. Figure 5 shows the results for t_p ranging from 0.01 to 10 s for $k^0 = 0.01$ cm/s. We see that the admittance gradually approaches the reversible behavior while the peak potential stays constant, when t_p gets longer. The reversibility depends on the observational time scale; the longer it is, the more reversible the result appears. This behavior is readily observed in cyclic voltammetric experiments.[25d]

The behavior described above can also be shown by the formalisms we used to obtain charge-transfer and mass-transfer admittance. When t is infinitely large in eqs 21-1, 21-2, and 21-3, both the charge and mass-transfer impedances approach those of reversible cases as can be seen from

$$\lim_{t \to \infty} R_{p,qr} = \frac{RT}{n^2 F^2 A k^0 C_O^*}$$
$$\cdot \frac{e^{\alpha nf[E(t)-E^{0'}]}}{\alpha\left(1 - \frac{k_f}{HD_O^{1/2}}\right) + (1-a)\frac{k_f}{HD_R^{1/2}}e^{nf[E-E^{0'}]}}$$

(24-1)

Substitution of eqs 3, 8-2, and 8-3 into eq 21-1 followed by a series of algebraic manipulations yields

$$\lim_{t \to \infty} R_{p,qr} = R_{p,rev}$$

(24-2)

In the same manner, we also obtain

$$\lim_{t \to \infty} Z_{w,qr} = Z_{w,rev}$$

(24-3)

Our simulation results also show the same evolution trends for k^0 ranging from 0.1 to 10^{-6} cm/s as shown in Figure 3.

4. Quasi-Reversible Systems: Effects of Diffusion Coefficients. Figure 6 shows the effect of the diffusion coefficient ranging 5×10^{-9} to 5×10^{-6} cm^2/s for $k^0 = 0.001$ cm/s and $t_p = 20$ ms. The admittances gradually approach the behaviors shown by the reversible case with no shift in peak potentials when diffusion coefficient decreases. This is obvious because the $k^0/D^{1/2}$ ratio becomes larger for a given k^0 value as the diffusion coefficient decreases, making the reaction pseudoreversible.[23] In other words, the mass transport cannot catch up with the rate of electron transfer in such a system. This is why many electrochemical reactions taking place in the solid state or polymer electrolytes look
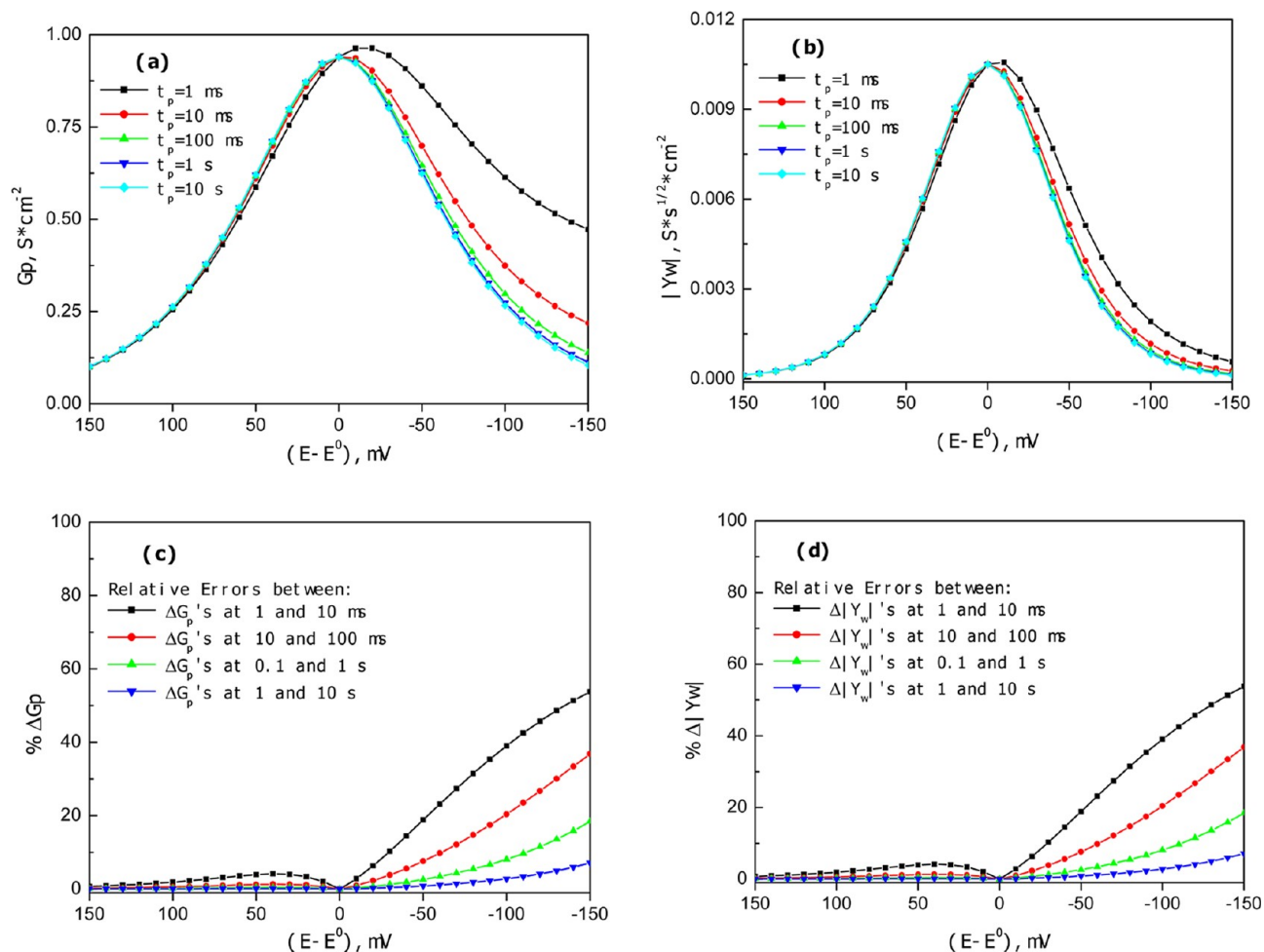
H

dx.doi.org/10.1021/jp306140w | *J. Phys. Chem. C* XXXX, XXX, XXX−XXX

Figure 10. (a) G_p and (b) Y_w vs η plots for t ranging from 1 ms to 10 s when $k^0 = 0.1$ cm/s and relative errors in (c) %ΔG_p and (d) %ΔY_w plotted vs η for t values of two neighboring decades.

Table 1. Lower (L) and Upper (U) Limits of the Time Span for Reliable Transient Impedance Measurements Depending on Exchange Rate Constants

k^0(cm/s)	10^1	10^0	10^{-1}	10^{-2}	10^{-3}	10^{-4}	10^{-5}	10^{-6}
τ_L(s)	10^{-4}	10^{-2}	10^0	10^2	10^4	10^6	10^8	10^{10}
τ_U(s)	10^{-12}	10^{-10}	10^{-8}	10^{-6}	10^{-4}	10^{-2}	10^0	10^2

reversible although their exchange rate constants fall in the irreversible category.[20j,33]

5. Quasi-Reversible Systems: Effects of Cathodic Charge-Transfer Coefficient.
Figure 7 shows the effects of the cathodic charge-transfer coefficient (α) ranging 0.30 to 0.90 for $k^0 = 0.001$ cm/s, $D = 5 \times 10^{-8}$ cm^2/s, $n = 1.0$, and $t_p = 20$ ms. The larger the coefficient, the more the G_p gradually deviates from the behaviors shown by the reversible case. Also, G_p increases significantly as α increases as well, which is readily expected. This is because the charge-transfer coefficient affects the symmetry of the crossing point of surface potential curves for the oxidant and reductant. For the Y_w, it is interesting to note that the peak appears at underpotential when $\alpha < 0.5$. Also, the peak Y_w values increases significantly for $\alpha > 0.5$.

6. Quasi-Reversible Systems: Effects of the Number of Electrons Transferred.
Figure 8 shows the effect of the number of electrons transferred ranging 1.0 to 3.0 for

$k^0 = 0.001$ cm/s, $D = 5 \times 10^{-8}$ cm^2/s, $\alpha = 0.5$, and $t_p = 20$ ms. It is readily expected that G_p increases with a faster slope for a larger n value as shown in Figure 8a. It is surprising, however, that the G_p values are greater than simply expected from their n values; this is perhaps because the concentration and therefore the mass transfer is not taken into account. The Warburg admittance values are also significantly affected as can be seen in Figure 8b. The half-widths of Y_w values are 112, 56, and 36 mV, respectively, for $n = 1-3$. Smaller k^0 values caused the half-peak widening. For a reversible case, this was constant with its value of $90.6/n$ mV.[6] This may serve as a criterion for the reversibility of an electrochemical reaction.

7. Measurable Time Windows.
Impedance measurements of an electrochemical system require that the system be stable, causal, finite, and linear.[2,3,10] Thus, the concept of the impedance requires that it be stable and independent of time and so does the impedance measurement during the data

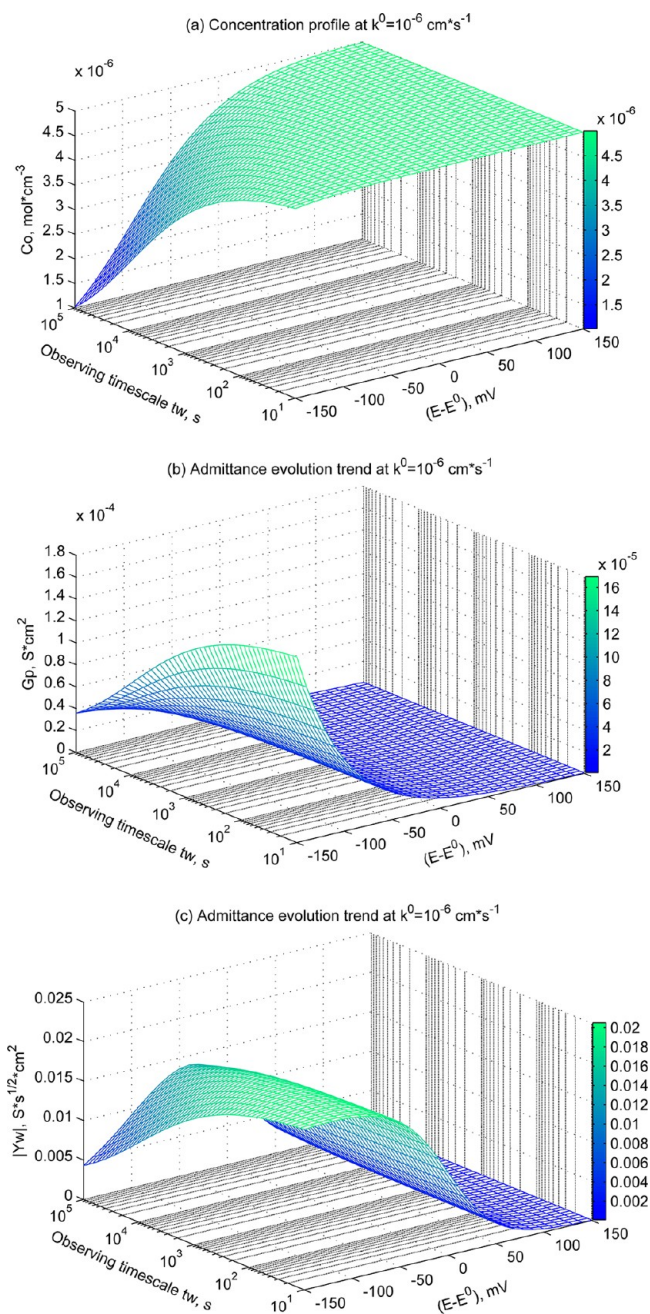J

dx.doi.org/10.1021/jp306140w | J. Phys. Chem. C XXXX, XXX, XXX–XXX

(a) Concentration profile at $k^0 = 10^{-6}$ cm*s^{-1}

(b) Admittance evolution trend at $k^0 = 10^{-6}$ cm*s^{-1}

(c) Admittance evolution trend at $k^0 = 10^{-6}$ cm*s^{-1}

Figure 11. (a) $C_O(x,t)$, (b) G_p, and (c) Y_w plotted as a function of t and η, for a reaction with $k^0 = 1 \times 10^{-6}$ cm/s and $D = 5 \times 10^{-6}$ cm^2/s.

observation period. For this reason, the traditional equipment for impedance measurements, such as the frequency response analyzer, waits until the current reaches a steady state by continuously monitoring the difference in currents (Δi) at times t_n and t_{n-1} after stepping a potential to a desired bias potential. Usually, however, an actual electrochemical system cannot reach a truly equilibrated state as long as the electrolysis proceeds and we assume that a steady state has been reached when the Δi value becomes smaller than the set value. We now discuss the data acquisition time span, during which the transient impedance measurements can be made by SCV-FTEIS experiment by achieving "pseudo" steady state and equilibrium conditions. During the period, the impedances

or admittances should stay reasonably constant within a certain range while measurements are being made continuously.

To set the basis of our discussion, we first show the changes in both concentration profile, $C_O(x,t)$, and admittances calculated employing eqs 20 and 21 for a reaction with $k^0 = 0.1$ cm/s as a function of experimental parameters, t (electrolysis time) and η, in Figure 9. We do not show $C_R(x,t)$ as it is just the complement of $C_O(x,t)$ when $D_O = D_R$. We see qualitatively from these plots that the concentration profile does not change too drastically for t at a given η. To examine the changes more quantitatively, we define the percentage of these changes for the change in t by an order of magnitudes, i.e., $\%\Delta G_{p,n} = \{|G_{p,n} - G_{p,n+1}|/G_{p,n+1}\} \times 100\%$ and $\%\Delta Y_{w,n} = \{|Y_{w,n} - Y_{w,n+1}|/Y_{w,n+1}\} \times 100\%$, where n indicates the order of magnitudes for t. The results of analysis are shown in Figure 10, where the relative differences are displayed for the neighboring decades in the t_p window. Panels c and d of Figure 10 indicate that differences are smaller than 10% even at $\eta = -150$ mV when $t_p > 1$ s. In other words, this is the *lower limit*, τ_L, of the observation time span for which a "pseudo" steady state can be observed. Here, 10% threshold seems not to be a very strict criterion; however, considering a 10-fold change in observation period, the threshold at 10% is still quite rigorous in terms of our test experiences. We examined for the exchange rate constants ranging 10 cm/s down to 10^{-6} cm/s and list corresponding τ_L values in Table 1. We find in this table that the step time (t_p) must be longer than 100 s for $k^0 = 0.01$ cm/s and it can be as long as 10^{10} s for $k^0 = 10^{-6}$ cm/s. This time scale is not practical at all for transient impedance measurements for slow reactions.

For slow charge-transfer processes, we need to take advantage of the *upper limit*, τ_U, instead. Figure 11 shows $C_O(x,t)$ and admittances for a slow electrochemical reaction with $k^0 = 10^{-6}$ cm/s. Here, the changes in concentration profiles and corresponding admittances are slower during smaller t values. The same parameters as shown in Figure 10 were obtained to evaluate the steadiness of the reaction and the results are shown in Figure 12. We now see that pseudosteady states are obtained even at a large $\eta = -150$ mV when t is smaller than τ_U, the upper limit of the observation time window, 10^2 s in this case. Again, the pseudo steady state impedances can be measured as long as the t_p is smaller than τ_U values listed in Table 1 for the reactions of various exchange rate constants.

We note from τ values in Table 1 that reliable results can be obtained by transient impedance measurements when t_p is either larger than τ_L or smaller than τ_U. Thus, from the practical point of view, we should use $t_p > \tau_L$ for faster reactions whereas $t_p < \tau_U$ for slower reactions. However, one should note that the reversibility of an electrochemical reaction depends on the rate of measurements; for example, a quasi-reversible reactions look reversible at slower scan rates whereas it becomes irreversible at higher scan rates in cyclic voltammetric experiments.[25d] In the SCV-FTEIS experiments, the reversibility is modulated by the ratio of the step height, ΔE, to the step period, t_p. Thus, one can make reliable transient impedance measurements for a variety of electrochemical reactions by properly choosing experimental parameters.
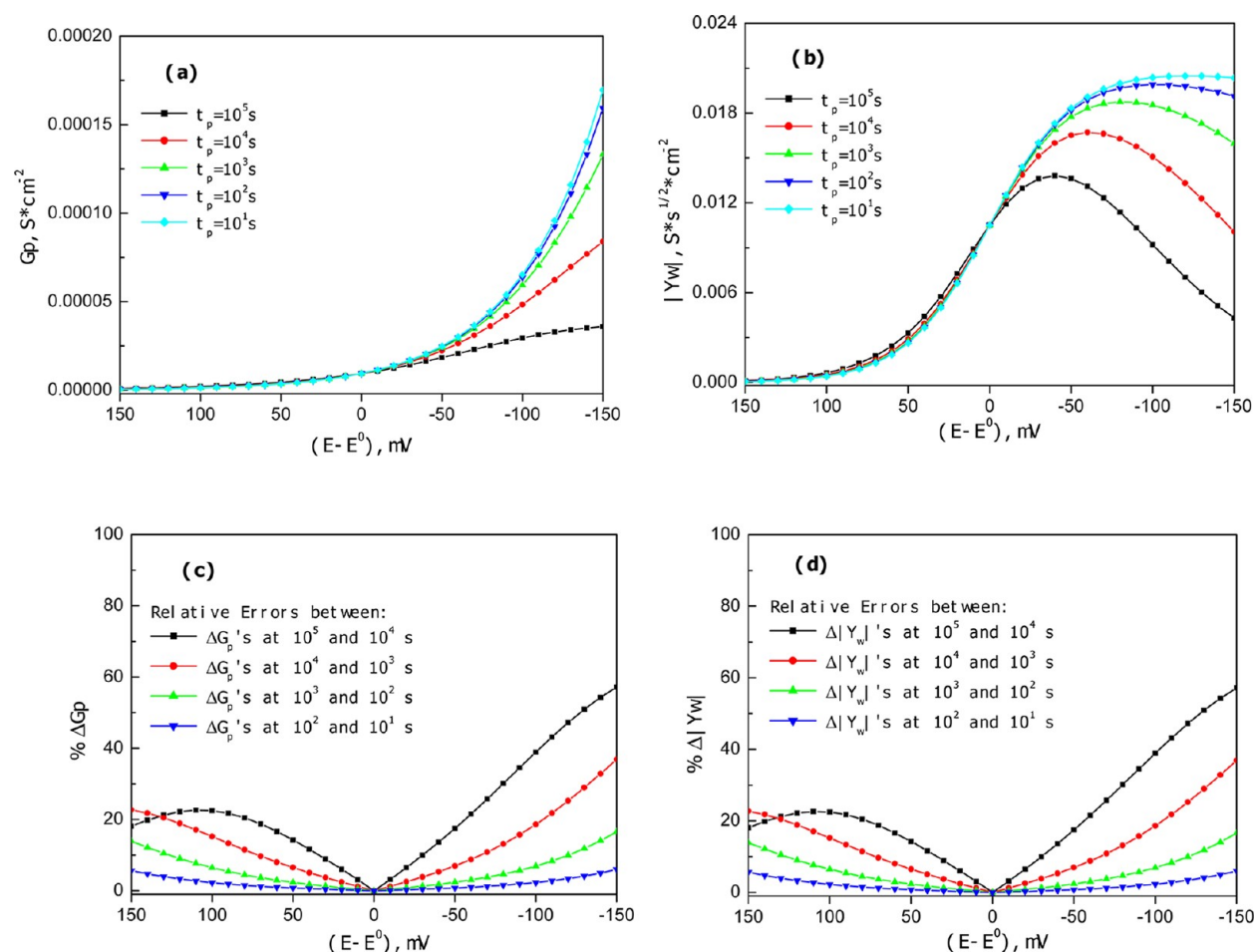
J

dx.doi.org/10.1021/jp306140w | J. Phys. Chem. C XXXX, XXX, XXX–XXX

Figure 12. (a) G_p and (b) Y_w vs η plots for t ranging from 10^1 to 10^5 s when $k^0 = 0.1$ cm/s and relative errors in (c) %ΔG_p and (d) %ΔY_w plotted vs η for t values of two neighboring decades.

■ CONCLUSIONS

In this work, we have worked out a unified model for transient faradaic EIS applicable to reversible, quasi-reversible, and irreversible charge-transfer reactions by deriving rigorous concentration equations for impedances. The Butler–Volmer kinetic relations were taken into account as a boundary condition for quasi-reversible systems. Simulation results employing the impedance equations show that k^0, D, n, α, and t_p directly affect the reversibility of electrode reaction. On the basis of the evolution trends of the admittance and conductance for different charge- and mass-transfer kinetic parameters including k^0, D, t, and η, their effects on the peak potential, E_p, and the half-peak width, $\Delta E_{p/2}$, of the Warburg admittances have been evaluated and discussed. As is the case for cyclic voltammetric experiments, E_p shifts in a negative direction while the $\Delta E_{p/2}$ value becomes broader in Warburg admittance voltammetric experiments. The same is true when a short t_p value is used or the scan rate is increased when the reaction falls in the quasi-reversible case. We have also presented the critical signal sampling time windows, τ_L and τ_U, for reliable transient impedance measurements depending on how facile the electrochemical reaction is. For reliable transient impedance measurements by using the SCV-FTEIS experiments, appropriate step heights and sampling periods should be selected.

How would one then obtain the kinetic parameters from the impedance measurements? When one obtains a set of impedance data at small potential intervals such as each 5, 10, or 20 mV from potentiodynamic impedance measurements employing the neo-FTEIS, a large body of R_p, C_d, and Y_W (double layer capacitance) data is obtained along with R_s (solution resistance) values (vide infra). The kinetic parameters such as k^0, α, and D values as well as a thermodynamic parameter ($E_{1/2}$ or E^0) are all obtained from the above set of data; details have been amply discussed in the recent literature.[4−6,20d,g−j,35,37]

Finally, we should point out that our work offers the basis for real-time transient monitoring of impedances employing a staircase cyclic voltammetry or "sampled-current voltammetry"[25c] experiment. The experiment provides not only a large body of impedance data as a function of potential[20,35] and/or time[36] but also cyclic voltammograms at scan rates of $\Delta E/t_p$. This is very important as the impedance data obtained in real time along with SCV/CVs provide the best way to reveal the very nature of the electrified interfaces while an electrochemical reaction proceeds. Given the simplicity of the SCV experiment and the amount of information it provides, we trust that it is time to shift the paradigm for electrochemical measurements from ever popular cyclic voltammetry to SCV experiments.

■ ASSOCIATED CONTENT

Ⓢ Supporting Information

List of nomenclature used in the paper. Derivation of eq 23. This information is available free of charge via the Internet at http://pubs.acs.org.

K

dx.doi.org/10.1021/jp306140w | J. Phys. Chem. C XXXX, XXX, XXX−XXX

AUTHOR INFORMATION

Corresponding Author
*E-mail: smpark@unist.ac.kr.

Present Address
†Faculty of Physics and Electronic Technology, Hubei University, Wuhan, Hubei 430062, PR China.

Notes
The authors declare no competing financial interest.

ACKNOWLEDGMENTS

REFERENCES

(1) Park, S.-M.; Yoo, J.-S. *Anal. Chem.* **2003**, *75*, 455A−461A.

(2) Barsoukov, E.; Macdonald, J. R. *Impedance Spectroscopy*; Wilely-Interscience: Hoboken, NJ, 2005.

(3) Orazem, M. E.; Tribollet, B. *Electrochemical Impedance Spectroscopy*; Wiley: Hoboken, NJ, 2008.

(4) Chang, B.-Y.; Park, S.-M. *Annu. Rev. Anal. Chem.* **2010**, *3*, 207−229.

(5) Chang, B.-Y.; Park, S.-M. *Anal. Chem.* **2007**, *79*, 4892−4899.

(6) Chang, B.-Y.; Lee, H. J.; Park, S.-M. *Electroanalysis* **2011**, *23*, 2070−2078.

(7) Macdonald, D. D. *Electrochim. Acta* **2006**, *51*, 1376−1388.

(8) Sluyters-Rehbach, M.; Sluyters, J. H. *J. Electroanal. Chem.* **1979**, *102*, 415−419.

(9) Popkirov, G. S.; Schneider, R. N. *Electrochim. Acta* **1993**, *38*, 861−867.

(10) (a) Stoynov, Z. B.; Savova-Stoynov, B. S. *J. Electroanal. Chem.* **1985**, *183*, 133−144. (b) Stoynov, Z. *Electrochim. Acta* **1992**, *37*, 2357−2359. (c) Stoynov, Z. *Electrochim. Acta* **1993**, *38*, 1919−1922.

(11) Savova-Stoynov, B.; Stoynov, Z. B. *Electrochim. Acta* **1992**, *37*, 2353−2355.

(12) (a) Creason, S. C.; Smith, D. E. *J. Electroanal. Chem.* **1972**, *36*, 1−7. (b) Creason, S. C.; Smith, D. E. *Anal. Chem.* **1973**, *47*, 2401−2403. (c) Smith, D. E. *Anal. Chem.* **1976**, *48*, 221A−240A and 517A−526A. (d) Schwall, R. J.; Bond, A. M.; Loyd, R. J.; Larsen, J. G.; Smith, D. E. *Anal. Chem.* **1977**, *49*, 1797−1805. (e) Schwall, R. J.; Bond, A. M.; Smith, D. E. *Anal. Chem.* **1977**, *49*, 1805−1812. (f) O'Halloran, R. J.; Schaar, J. E.; Smith, D. E. *Anal. Chem.* **1978**, *50*, 1073−1079. (g) Crzeszczuk, M.; Smith, D. E. *J. Electroanal. Chem.* **1983**, *157*, 205−219.

(13) Popkirov, G. S.; Schindler, R. N. *Rev. Sci. Instrum.* **1992**, *63*, 5366−5372.

(14) Ragoisha, G. A.; Bondarenko, A. S. *Electrochem. Commun.* **2003**, *5*, 392−395.

(15) (a) Darowicki, K.; Slepski, P. *J. Electroanal. Chem.* **2003**, *547*, 1−8. (b) Darowicki, K.; Orlikowski, J.; Arutunow, A. *Electrochim. Acta* **2003**, *48*, 4189−4196.

(16) Pettit, C. M.; Goonetilleke, P C.; Sulyma, C. M.; Roy, D. *Anal. Chem.* **2006**, *78*, 3723−3729.

(17) Gabrielli, C.; Keddam, M.; Lizee, J. F. *J. Electroanal. Chem.* **1986**, *205*, 59−75.

(18) Mochalov, S. E.; Kolosnitsyn, V. S. *Instrum. Exp. Technol.* **2000**, *43*, 53−56.

(19) Yoo, J.-S.; Park, S.-M. *Anal. Chem.* **2000**, *72*, 2035−2041.

(20) (a) Yoo, J.-S.; Song, I.; Lee, J.-H.; Park, S.-M. *Anal. Chem.* **2003**, *75*, 2962−2968. (b) Chang, B.-Y.; Hong, S.-Y.; Yoo, J.-S.; Park, S.-M. *J. Phys. Chem. B* **2006**, *110*, 19386−19392. (c) Park, J.-B.; Chang, B.-Y.; Yoo, J.-S.; Hong, S.-Y.; Park, S.-M. *Bull. Korean Chem. Soc.* **2007**, *28*, 1523−1530. (d) Hong, S.-Y.; Park, S.-M. *J. Phys. Chem. B* **2007**, *111*, 9779−9786. (e) Chang, B.-Y.; Ahn, E.; Park, S.-M. *J. Phys. Chem. C* **2008**, *112*, 16902−16909. (f) Mozaffari, S. A.; Chang, T.; Park, S.-M. *J. Phys. Chem. B* **2009**, *113*, 12434−12442. (g) Park, J.-B.; Park, S.-M. *J. Electroanal. Chem.* **2011**, *656*, 243−251. (h) Min, G. G.; Kim, S. B.; Park, S.-M. *J. Electrochem. Soc.* **2011**, *158*, F92−F99. (i) Cho, S. H.;

Lee, H. J.; Ko, Y.; Park, S.-M. *J. Phys. Chem. C* **2011**, *115*, 6545−6553. (j) Min, G. G.; Ko, Y.; Kim, T.-H.; Song, H.-K.; Kim, S. B.; Park, S.-M. *J. Electrochem. Soc.* **2011**, *158*, A1267−A1274.

(21) Delahay, P. *J. Am. Chem. Soc.* **1953**, *75*, 1430−1435.

(22) Randles, J. E. B. *Discuss. Faraday Soc.* **1947**, *1*, 11−19.

(23) Chang, B.-Y.; Park, S.-M. *Anal. Chem.* **2006**, *78*, 1052−1060.

(24) Lasia, A. In *Modern Aspects of Electrochemistry*; Kluwer Academic/Plenum Publications: New York, 1999; Vol. 32, Chapter 2, p 143.

(25) Bard, A. J.; Faulkner, L. R. *Electrochemical Methods*, 2nd ed.; Wiley: New York, 2001; (a) Chapter 10, (b) Chapter 3, (c) Chapter 5, (d) Chapter 6.

(26) Karris, S. T. *Circuit Analysis II with MATLAB*; Orchard Publications: Fremont, CA, 2009.

(27) (a) Seralathan, M.; Osteryoung, R. O.; Osteryoung, J. G. *J. Electroanal. Chem.* **1987**, *222*, 69−100. (b) Bilewicz, R.; Wikiel, K.; Osteryoung, R.; Osteryoung, J. **1989**, *61*, 965−972.

(28) Foresti, M. L.; Guidelli, R.; Nyholm, L. *J. Electroanal. Chem.* **1989**, *269*, 27−40.

(29) Poularikas, A. D. *The Electrical Engineering Handbook Series: The handbook of formulas and tables for signal processing*; CRC Press LLC: Boca Raton, FL, 1999.

(30) Jurczakowski, R.; Lasia, A. *Anal. Chem.* **2004**, *76*, 5033−5038.

(31) Koutecky, J. *Collect. Czech. Chem. Commun.* **1953**, *18*, 597−610.

(32) Weber, J.; Koutecky, J. *Collect. Czech. Chem. Commun.* **1955**, *20*, 980−9831.

(33) Cha, D. K.; Park, S.-M. *J. Electroanal. Chem.* **1998**, *459*, 135−144.

(34) Osteryoung, J. *Acc. Chem. Res.* **1993**, *26*, 77−83.

(35) Ko, Y.; Park, S.-M. *J. Phys. Chem. C* **2012**, *116*, 7260−7268.

(36) (a) Park, J.-Y.; Lee, Y.-S.; Chang, B.-Y.; Karthikeyan, S.; Kim, K. S.; Kim, B. H.; Park, S.-M. *Anal. Chem.* **2009**, *81*, 3843−3850. (b) Park, J.-Y.; Lee, Y.-S.; Chang, B.-Y.; Kim, B. H.; Jeon, S.; Park, S.-M. *Anal. Chem.* **2010**, *82*, 8342−8348. (c) Huang, X.; Chen, H.; Deng, H.; Wang, L.; Liao, S.; Tang, A. *J. Electroanal. Chem.* **2011**, *657*, 158−163.

(37) Gulaboski, R.; Ferreira, E. S.; Pereira, C. M.; Cordeiro, M. N. D. S.; Garau, A.; Lippolis, V.; Silva, A. F. *J. Phys. Chem. C* **2008**, *112*, 153−161.